Supplementary Information

Monolithic additive manufacturing of fluid-structure coupled architected cellular mechanical system for rate-adaptive enhanced energy dissipation

Jawad Ahmad , Valerii Zudov, Mayur Jiyalal Prajapati, Marat Dosaev, Bing Joe Hwang, Wei-Nien Su, Cho-Pei Jiang, Jeng-Ywan Jeng *

Section S1: Abaqus Simulation

The CMS was modeled using Abaqus/CAE © 2024 to numerically simulate the actual experimental compression setup. The unit cell CMS was meshed with modified linear tetrahedron element (C3D4) with a mesh size of 1 mm while the fluid domain was meshed with 0.9 mm. TPU was modeled as a hyperelastic material (density= 1.12×10^{-9} Tons/mm^{-3}) and based on the tensile test conducted on dog-bone specimen, the second order Ogden strain energy density function was chosen for it. The silicon oil was treated as a nearly incompressible inviscid Newtonian fluid using continuum pseudo particles (PC3D elements) using SPH approach. Its density was 9.4×10^{-10} Tons/mm^{-3}, viscosity 1×10^{-6} MPa.s, speed of sound (c_0= 9.85×10^5 mm s^{-1}) and Hugoniot coefficient S=0, Gruneisen parameter Γ_0=0. Analytical rigid plates were chosen at the top and bottom boundaries with tangential penalty (Friction Coefficient=0.3) and hard normal contact to replicate the experimental compression conditions. The bottom plate was fixed while top plate was moved downward for compression.

Section S2: Mechanical response under quasi static compression

Table S2.1 Quasi-static flow regime and times scale analysis

Parameter	Value	Parameter	Value
Orifice diameter	1.5mm, 3.0mm	Orifice length	0.669 mm
ρ (water)	1000 kg/m^3	ρ (silicone oil)	970 kg/m^3
μ (water) 0.001 Pa. s	$\upsilon=1.0\times10^{-6}$ m^2/s	μ (0.1 Pa. s silicone oil)	$\upsilon=1.031\times10^{-4}$ m^2/s
μ (1.0 Pa. s silicone oil)	$\upsilon=1.031\times10^{-3}$ m^2/s	Δx	8.5 mm

Table S2.2 Reynolds number (*Re*=ρvd/μ) for d=1.5 mm

Speed (mm/min)	V (mm/s)	*Re* (water)	*Re* (0.1 Pa. s)	*Re* (1.0 Pa. s)
10	0.166	0.25	2.43×10^{-3}	2.43×10^{-4}
500	8.33	12.5	0.12	0.012
1000	16.66	25	0.24	0.024

Table S2.3 Reynolds number (*Re*=ρvd/μ) for d=3.0 mm

Speed (mm/min)	V (mm/s)	*Re* (water)	*Re* (0.1 Pa. s)	*Re* (1.0 Pa. s)
1000	16.66	50	0.49	0.049

Table S2.4 Viscous diffusion time scale: $\tau_{viscous}$= d^2/υ

Fluid	$\tau_{viscous}$ (s) for d=1.5 mm	$\tau_{viscous}$ (s) for d=3.0 mm
1.0 Pa. s	2.18×10^{-3}	8.73×10^{-3}
0.1 Pa. s	2.18×10^{-2}	8.73×10^{-2}
water	2.25	9

Table S2.5 Time scale ratio: $\tau_{viscous}$/ $\tau_{compression}$ (d=1.5 mm)

Fluid	$\tau_{compression}$ at 10 mm/min	Ratio	$\tau_{compression}$ at 1000 mm/min	Ratio
1.0 Pa. s	51	4.3×10^{-5}	0.51	0.0043
0.1 Pa. s	51	4.3×10^{-4}	0.51	0.043
water	51	0.044	0.51	4.41

Table S2.6 Time scale ratio: $\tau_{viscous}$/ $\tau_{compression}$ (d=3.0 mm)

Fluid	$\tau_{compression}$ at 10 mm/min	Ratio	$\tau_{compression}$ at 1000 mm/min	Ratio
1.0 Pa. s	51	1.71×10^{-4}	0.51	0.0171
0.1 Pa. s	51	1.71×10^{-3}	0.51	0.171
water	51	0.176	0.51	17.6

Table S2.7: Energy Metrics

Sample Type	Compression Speed (mm/min)	*K (N/mm)*	F_{peak} *(N)*	*EA (mJ)*	*SEA (mJ/g)*
Empty	10	71.64	624.52	2270	113.5
	50	73.78	656.53	2406	120.3
	100	75.76	670	2421	121.05
	250	81.56	694.35	2563	128.15
	500	82.16	765.46	2784	139.2
	750	82.55	848.44	3052	152.6
	1000	84.96	980.74	3523	176.15
Filled	10	74.98	736.55	2628	100.03
	50	78.18	747.53	2726	103.76
	100	80.85	768.5	2853	108.60
	250	85.0	822.09	3131	119.18
	500	90.63	896.63	3509	133.57
	750	95.16	979.25	3930	149.60
	1000	102.21	1099.89	4612	175.56

Table S2.8: Damping Metrics

Sample Type	Compression Speed (mm/min)	*ED (mJ)*	*SED (J/kg)*	*Loss factor (ζ)*	F_d $=F_{load}$-F_{unload} @ 6mm
Empty	10	328	16.4	0.023	42.65
	50	368	18.4	0.024	47.62
	100	381	19.05	0.025	48.55
	250	400	20	0.025	53.54

	500	438	21.9	0.025	60.06
	750	495	24.75	0.026	69.48
	1000	634	31.7	0.028	84.1
	10	379	14.42	0.022	47.81
	50	470	17.89	0.027	63.2
	100	576	21.92	0.032	81.89
Filled	250	825	31.40	0.041	133.4
	500	1135	43.20	0.051	199.9
	750	1413	53.78	0.057	253.03
	1000	1799	68.48	0.062	302.81

Section S3: Mechanical response under dynamic compression

Table S3.1 Dynamic flow regime and times scale analysis

Reynolds number under dynamic loading (1.0 Pa. s, d=1.5 mm)

Parameters (ρ= 970 kg/mm^3), μ=1.0 Pa. s, A=0.00425)

Frequency (Hz)	V (m/s)	Re
1.0	0.0267	0.039
2.5	0.068	0.097

Table S3.2 Time scale ratio: $\tau_{viscous}$/ $\tau_{compression}$ (d=1.5 mm)

Frequency (Hz)	T/2 (s)	$\tau_{viscous}$ (s) for d=1.5 mm	Ratio
1.0	0.5	2.18×10^{-3}	4.37×10^{-3}
2.5	0.2	2.18×10^{-3}	1.09×10^{-2}

Table S3.3 Time scale ratio: $\tau_{viscous}$/ $\tau_{compression}$ (d=3.0 mm)

Frequency (Hz)	T/2 (s)	$\tau_{viscous}$ (s) for d=3.0 mm	Ratio
1.0	0.5	8.73×10^{-3}	1.75×10^{-2}
2.5	0.2	8.73×10^{-3}	4.37×10^{-2}

Table S3.4 Dynamics Metrics for 6th cycle

Sample Type	Frequency (Hz)	F_{max}(N)	ED (mJ)	SED (mJ)	ζ
	1.0	701.66	442.54	22.19	0.028
Empty	2.5	792.49	521.02	26.44	0.033
	1.0	790.98	995.09	37.87	0.058
Filled	2.5	1086.90	1391.96	52.98	0.061

65 Table S3.5 Comparative benchmark of the present CMS against prior related works

Reference	Structure	Mechanism	Rate-adaptive	Fabrication/ assembly	Cyclic stability	Key limitation
Corvi & Collini et al. [1]	STF filled TPMS	Bulk STF presence	i) Peak acceleration reduction ii) Energy absorption enhancement by 85% at high strain rates	3D printing + manual fluid injection	Not tested	No benefit under quasistatic or low frequency loading, no loss factor reported
Shi et al. [2]	PA12-ONSH dome	Orifice flow	EA=100-150 mJ at 1-6 mm/s	Manual assembling	Tested for 18 cycles	Require assembly and sealing
Li et al. [3]	Interwind friction based	Dry friction	EA≈10 Kj/kg	Manual assembling	>200 cycles	Wear of sliding interfaces, multi-component assembly
Prajapati et al [4]	Closed cell lattice	Bulk silicon oil present, no directed flow	EA=60-118 J (quasi-static)	Combined printing and filling	no cyclic durability data	No dedicated orifice, no cyclic durability data, no velocity proportional damping
Ye H et al. [5]	CIS multi-material lattice	Structural compression only	SEA=126 J/kg/cycle	Combined printing	>500 cycles	No rate adaptivity reported
Present CMS	Corrugated cellular structure	Orifice-governed viscous flow	SED=68.48 J/kg Loss	Single-step additive manufacturin	>400 cycles for dynamic testing against multiple	----

	factor= 0.062	g	frequencies

Section S4: Phenomenological Model

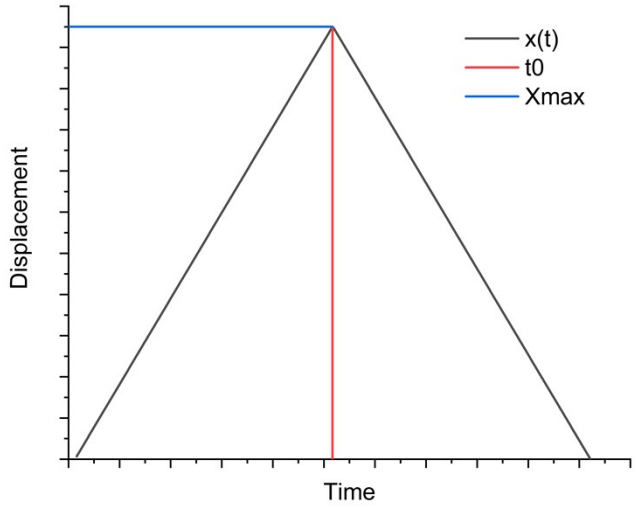

Figure S1: Experimental displacement-time profile

S4.1: Empty Configuration (Coefficients detail)

$$k_1\left(1+e^{\frac{-k_1x^2}{c_1 l|\dot{x}|}}\right)^2\dot{x}$$

- The $k_1\left(1+e^{\frac{-k_1x^2}{c_1 l|\dot{x}|}}\right)^2\dot{x}$ describes the linear elastic and plateau regions of the loading curve and may be analogous to the Maxwell model, having a nonlinear viscous dashpot connected in series with a linear spring element [6,7], where the fractional exponent indicates the dashpot nonlinearity[8]. The parameter k_1 governs the inclination of the linear elastic region, while parameter c_1 controls the load level and slope of the plateau region (Figure S2-a,d). Such influence (the same as in the article [9] clearly refers to stiffness and viscosity, respectively, which may confirm the proposed spring-damper scheme of this part.

- The term $k_2\left(-1+e^{\frac{\gamma}{l}x}\right)^4\dot{x}$ describes the densification region and is analogous to a nonlinear spring [9]. The γ is a dimensionless coefficient and together with the bracketed component governs the onset position and slope of the densification region, as shown in Figure S2-b, where k_2 carries the dimensions of the spring stiffness.

- The term $\left(-k_3+k_4e^{\frac{-c_2}{k_4 l_s}|\dot{x}|}\right)\dot{x}$ is responsible for improving the accuracy of the model across

the full range of compression speed, particularly at low and high speeds. Its form bears analogy to the Generalized Maxwell model [10] or Standard Linear Solid model (Maxwell representation) [11,12]. The negative sign of the stiffness may be represented as a spring positioned at a defined inclination angle, as in the articles [13,14].

- The term $\tau_1|\dot{x}|F$ governs hysteresis work, a larger value of τ_1 directly increases the enclosed hysteresis loop area (Figure S2-c).

A parametric sensitivity analysis was performed to establish the physical correspondence of each parameter, and the results are presented in Figure S2. For case (a), the parameter c_1 included in the term $\mathrm{k}_1\left(1+e^{\frac{-k_1x^2}{c_1l|\dot{x}|}}\right)^2\dot{x}$ is a constant corresponding to the value in Table 3, the same for k_1 in (d), for γ in (b) and k_2 in (e). For cases (a-d), all other parameters except the one under investigation are set to zero, isolating each individual parameter contribution to the curve shape. For case (c), all parameters except τ_1 retain their values mentioned in Table 3. For this representation, a single loading velocity was selected to have consistency across all cases (a-e). The parameter values were selected as follows: $c_1' < c_1'' < c_1''' < c_1'''' < c_1'''''$ (relevant for the rest as well: $\gamma^{(i)} < \gamma^{(i+1)}$, $\tau_1{}^{(i)} < \tau_1{}^{(i+1)}$, $k_1{}^{(i)} < k_1{}^{(i+1)}$, $k_2{}^{(i)} < k_2{}^{(i+1)}$).

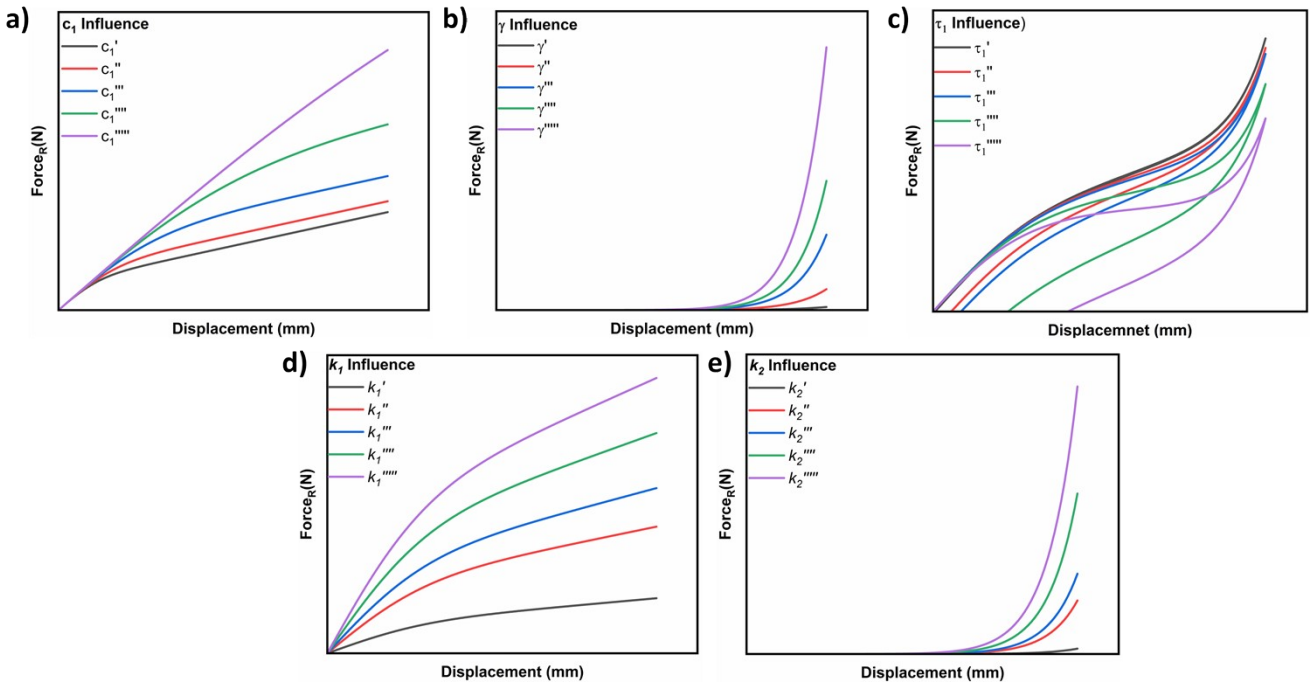

Figure S2: Parametric sensitivity of the constitutive model on the force-displacement curve shape **(a)** influence

of c_1, **(b)** influence of γ, **(c)** influence of τ_1, **(d)** influence of k_1, **(e)** influence of k_2.

S4.2: Filled Configuration (Coefficients detail)

- The term $\frac{k_5}{l_s}x|\dot{x}|$ primarily governs the hysteresis contribution in the filled configuration, probably analogous to a nonlinear spring [15], where increasing k_5 enhances the hysteresis loop area. At the same time, the negative sign of the parameter may indicate an element with negative stiffness, which is located at a certain angle [2,13,14].

- The exponential term $k_6 e^{-\frac{\alpha_1}{l_s^2}(x-l_1)^2}$ captures the localized force amplification in the loading curve and its influence observed during unloading as well, and is analogous to a part of the Carreau-Yasuda model [16]. The coefficient k_6 controls the magnitude of the jump in the curve, while α_1 governs its smoothness. These are highly influential parameters and are related to the fluid properties, especially α_1 is related to the fluid viscosity. The value α_1, in this case, is equal to the value of (without dimension) k_6 divided by the dynamic viscosity value Ps value squared (in this case, the liquid is Silicon oil 1.0 Pa.s=1000 cPs (10Ps)), that is $\alpha_1 = \frac{75}{10^2} = 0.75.$ l_s is the thickness of the corrugated section, which is equal to $l_s = 1.0\ mm$. Here the term $l_1 = h_d - n \cdot h_{gr} + r_0$ defines the onset of the slope in the curve, where h_{gr} is the internal height of one corrugated section part (~5.32 mm), n is the number of grooves and r_0 is the orifice height (~0.669 mm).

- The term $\left(k_7 + k_8 e^{-\frac{\alpha_2}{l_s^2}(x-l_2)^2}\right)\dot{x}$ represents a combination of linear and nonlinear springs associated with the progressive engagement of a filled corrugated compliant section. The coefficients k_8, α_2 and l_2 have the same meaning and influence on the curve as k_6, α_1 and l_1. The value (without dimensions) $\alpha_2 = k_8 K$, where K coefficient of expansion (~ 0.00096) and $l_2 = \sqrt[3]{V_{ch}} - l_a$ (~9.4 mm),where V_{ch} is the volume of the chamber, and l_a is the thickness of the accumulator section. The values of the k_8 coefficient depends on the volume of the liquid.

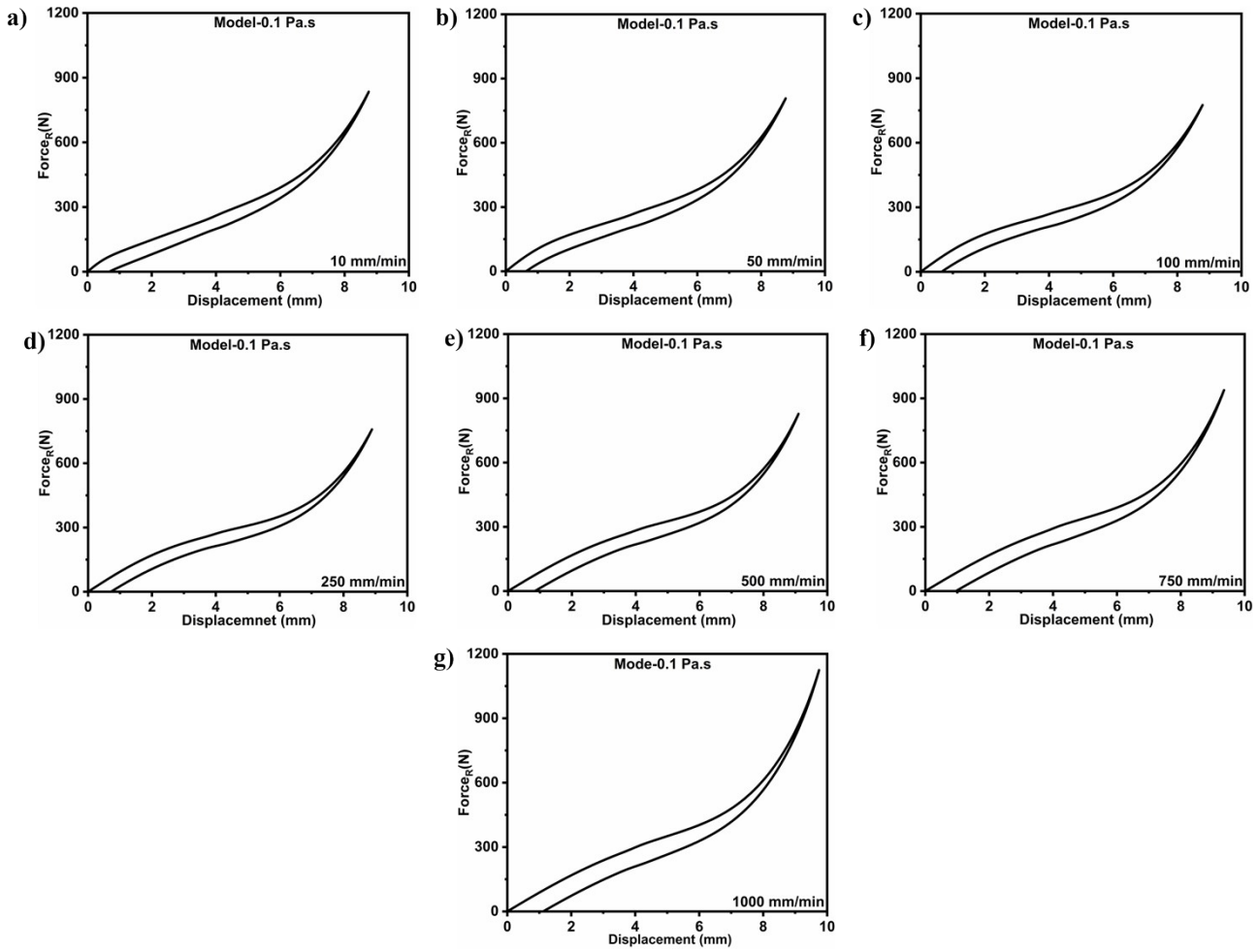

Figure S3: Response of filled configuration model with reduced viscosity across the quasi static test range 10-1000 mm/min (a-g).

Section S5: Video of Single-step manufacturing approach

The CMS was monolithically fabricated using a multi-extruder printer, wherein a dedicated filament extruder and a fluid dispensing extruder operate within a single automated print cycle without human intervention. As illustrated in movie S1-DDM-MOV, upon completion of designated lattice layer, the filament extruder is parked at its docking site, and the fluid dispensing extruder is automatically engaged to deposit a controlled volume of silicon oil within the cellular cavities. Upon completion of fluid deposition, the dispensing extruder is docked and the filament extruder resumes structural printing of subsequent layers. This automated tool-switching protocol enables the direct encapsulation of silicon oil within the CMS during fabrication, eliminating the post-processing, manual filling and is fully consistent with the principles of direct digital manufacturing.

S1-DD-Edited.mp4

References

1 A. Corvi and L. Collini, *Mater. Des.*, DOI:10.1016/j.matdes.2024.113174.

2 W. Shi, S. Yue, D. Shu, Y. Yuan, Z. Du and G. Gao, *Constr. Build. Mater.*, DOI:10.1016/j.conbuildmat.2025.140297.

3 J. Li, Z. Chen, Q. Li, L. Jin and Z. Zhao, *Advanced Science*, DOI:10.1002/advs.202105769.

4 M. J. Prajapati, A. Kumar and J. Y. Jeng, *Adv. Mater. Technol.*, DOI:10.1002/ADMT.202500446.

5 H. Ye, X. Huang, L. Jin, S. Zhou, G. Xie, Z. Hu, R. Li, H. Mo, S. Fang, W.-H. Liao, Q. Ge and X. Song, *Virtual Phys. Prototyp.*, DOI:10.1080/17452759.2026.2637380.

6 G. C. Papanicolaou and S. P. Zaoutsos, in *Creep and Fatigue in Polymer Matrix Composites (Second Edition)*, ed. R. M. Guedes, Woodhead Publishing, Second Edition., 2019, pp. 3–59.

7 R. M. Christensen, *Theory of Viscoelasticity*, 1982, 1–34.

8 P. A. Lukash, *Moscow: Stroiizdat*.

9 V. Goga and B. Hučko, *Journal of Mechanical Engineering*, 2016, **65**, 5–20.

10 D. Roylance, *ENGINEERING VISCOELASTICITY*, 2001.

11 C.-Y. Lin and Y.-C. Lin, *Journal of Experimental and Theoretical Physics*, 2024, **139**, 11–28.

12 C.-Y. Lin, *Mechanics of Advanced Materials and Structures*, 2024, **31**, 2370–2385.

13 T. Liu, R. Deng, L. Jin and J. Cai, *Int. J. Mech. Sci.*, 2024, **283**, 109664.

14 A. Guell Izard, R. Fabian Alfonso, G. McKnight and L. Valdevit, *Mater. Des.*, 2017, **135**, 37–50.

15 Solid Mechanics Part I, https://pkel015.connect.amazon.auckland.ac.nz/SolidMechanicsBooks/Part_I/index.html, (accessed 18 March 2026).

16 L. P. Martínez-Padilla, *John Wiley and Sons Inc*, 2024, preprint, DOI: 10.1111/jtxs.12802.